Structure, defects and strain in silicon-silicon oxide interfaces

Goran Kovačević, Branko Pivac*

Department of materials physics, Rudjer Boskovic Institute, Bijenička 56, P.O.B. 180, HR-10002 Zagreb, Croatia

Tel, fax: +385 01 4561486

gkova@irb.hr

KEYWORDS: Silicon, silicon oxide, interface, defect, strain

ABSTRACT:

The structure of the interfaces between silicon and silicon-oxide are responsible for proper functioning of MOSFET devices while defects in the interface can deteriorate this function and lead to theirs failure. In this paper we modeled this interface and characterized its defects and strain. MD simulations were used for reconstructing interfaces into a thermodynamically stable configuration. In all modeled interfaces, defects were found in form of three-coordinated silicon atom, five coordinated silicon atom, threefold-coordinated oxygen atom or displaced oxygen atom. Three-coordinated oxygen atom can be

created if dangling bonds on silicon are close enough. The structure and stability of three-coordinated silicon atoms (P_b defect) depend on the charge as well as on the electric field across the interface. The negatively charged P_b defect is the most stable one, but the electric field resulting from the interface reduces that stability. Interfaces with large differences in periodic constants of silicon and silicon oxide can be stabilized by buckling of silicon layer. Mechanical stress resulted from the interface between silicon and silicon oxide is greater in the silicon oxide layer. *Ab-initio* modeling of clusters representing silicon and silicon oxide shows about three time larger susceptibility to strain in silicon oxide than in silicon if exposed to the same deformation.

Introduction

Silicon is an intrinsic semiconductor which can be technologically produced in the most pure form as a single element. Its electronic properties can be fine-tuned in the wide range by intentional doping with specific elements.[1] Moreover, surface-oxidation produces a silicon dioxide (SiO_2); a stable and uniform material with large band gap, which can serve as a high quality insulator. Modern techniques succeed in producing precise, atomically flat surfaces of silicon[1,2], covered with SiO_2 layer, only several atomic layers thick.[3]

These properties make silicon a unique element, suitable for building metal-oxide semiconductor field-effect transistor (MOSFET)[4], a *building-block* device for explosive development of information and communication technologies in the several last decades. Therefore it makes the interface between silicon and SiO_2 (Si-SiO_2) technologically one of the most important atomic interfaces.[5] Properties of MOSFET devices are greatly influenced by the Si-SiO_2 interface since charged defects that might be

present there could significantly alter its properties, therefore understanding the structure and defects at Si-SiO_2 interfaces is important for further development of electronic devices, especially with constant shrinking of the SiO_2 thickness.[4,6] While silicon, used in manufacture of electronic devices is crystalline, thermally grown SiO_2 is amorphous[6,7] and the interface is abrupt and smooth[8]. Nevertheless, there are indications about the ordered crystalline structure of the SiO_2 close to the Si–SiO_2 interface.[8-11]

At the interface region, there should be at least one layer of silicon atoms that are bonded both with oxygen and silicon atoms. These silicon atoms are in intermediate oxidation states (+1, +2, +3, depending on the number of oxygen atoms they are bound to).[12,13] The presence of these silicon atoms with intermediate states is referred as a chemical stress[14] while mismatch in periodic constants is a source of the mechanical stress.[8,11,15,16] The interface layer is also found to be a source of structural defects that are electrically active and are responsible for degradation of performances of MOS devices upon exposure to high electrical currents or ionizing radiation. The most important one is the P_b defect.[17-19] It is identified as a silicon atom with a dangling bond [Si(3)].[15,20-22] The presence of this defect is easily identified with the EPR spectroscopy.[23] Si(3) is amphoteric, i.e. it can be present in positive [$Si(3)^+$], neutral [$Si(3)^0$] and negative state [$Si(3)^-$].[24] Their population depend on their energy, relative to the Fermi level. Since only $Si(3)^0$ is paramagnetic, only this species is detected in EPR spectra. $Si(3)^0$ has an energy in the mid-gap, between valence and conductive bands of silicon. Increasing or lowering the Fermi level, extinguishes the EPR signal since $Si(3)^0$ is being depopulated. According to Lenahan and Conley[23], $Si(3)^+$ has lower and $Si(3)^-$ has higher energy relative to $Si(3)^0$.

Despite tremendous importance and intensive studies on the interface between these two materials, there are still many unknowns in the structure of that interface. In our previous paper[25], we took five models for the interfaces between the silicon [100] surface and different forms of silicon oxide and

challenged them by simulating an exposure to high temperatures and slowly cooling them down. Chosen temperatures were high enough to alter the bonding pattern in strained bonds at interfaces, but too low for melting either silicon or silicon oxide. The procedure of heating and slowly cooling was used in order to drive system toward the energetically more stable state.

In this paper our aim is to characterize interfaces with other silicon surfaces ([110] and [111]) and investigate strain and defects that are the result of interfacing. Models for interfaces with Si[110] and Si[111] were created for β-cristobalite (βc) and β-quartz (βq) silicon oxide forms.

Computational methods

We used the Reax force field (ReaxFF)[26] to model and characterize interfaces between Si [110] and [111] surfaces and different phases of crystalline and amorphous SiO_2. While traditional force fields have restrictions on a very narrow part of potential energy surfaces, close to energy minima, the ReaxFF was designed to accurately describe geometries that are far from the equilibrium including processes such as bond breaking, molecular isomerization, change of atom coordination or change in molecular conformation. In this work, we used parameters, developed by van Duin at al.[27,28] for silicon and silicon oxide systems ($ReaxFF_{SiO}$). This force field was parameterized against accurate quantum chemical and periodic DFT calculations and can describe cases where oxygen and/or silicon is under- or over-coordinated or systems with silicon involved in double or triple bonds. The ability of the $ReaxFF_{SiO}$ force field to predict stability of polymorphs of SiO_2 was also demonstrated.[27]

Model systems were created by positioning a silicon slab against crystalline silicon oxide layers. Orthorhombic supercells of silicon and silicon oxide were obtained by cutting their lattices to the sizes

that have approximate match. Interfaces with Si[100] surfaces were the subject of our previous paper[25], while interfaces with Si[110] and Si[111] are constructed *de-novo*.

All layers were compressed or expanded along appropriate directions in order to achieve exact matching in the lattice constants of both silicon and silicon oxide. Silicon and/or silicon oxide layers were translated in directions perpendicular to the direction of stacking in order to achieve optimal bonding between layers. Periodic boundary conditions were applied during the process of translation in order to keep all atoms in the unit cell. Bonding is further adjusted by dislocating some atoms in the interface to optimal positions. If possible, the presence of unsatisfied valencies was eliminated by insertion of oxygen atoms.

Such prepared systems were subjected to a series of geometry optimizations and low-temperature molecular dynamics (MD) simulations. Geometry optimization relaxes the system by reducing forces acting on atoms and low temperature MD simulations are used to relax system by changing unit cell parameters. After relaxation, the temperature of the silicon oxide layers was increased to 1000 K over 15 ps. The temperature of 1000 K is too low for melting the silicon or any of silicon oxide forms considered, but is high enough for atom rearrangements to take place in the Si–SiO_2 interface region. The MD simulation was performed on the system for 50 ps after which, the system was cooled for another 50 ps at the cooling rate of 1.94 10^{13} K s^{-1}. Geometry optimization was performed on the final geometry. Periodic boundary conditions were applied in all three dimensions. The time integration step of 0.5 fs was used with the velocity-Verlet integrator in all MD steps. The temperature and the pressure were maintained with the Nose–Hoover thermostat/barostat. The pressure of 1 atmosphere was kept in all MD steps. All MD calculations were done with the LAMMPS program package.

The interfaces between Si[100], Si[110] and Si[111] and amorphous SiO_2 ($aSiO_2$) are also constructed. The methodology for obtaining $aSiO_2$-Si-$aSiO_2$ systems is different from the methodology

used in construction interfaces between silicon and crystalline SiO_2 ($cSiO_2$).[29,30] First, the sample of amorphous SiO_2 was constructed by simulation of heating the sample of β tridymite. β tridymite is chosen since it's density is close to the density of $aSiO_2$.[30] The periodic constants of the unit cell were adjusted in order to exactly match the density of $aSiO_2$ (2.20 g cm^{-1}). The system was heated from 0 K to 3500 K over 5 ps. After that, the temperature of 3500 K was maintained for next 5 ps. In that period, atoms moved from their initial positions and mixed. The system was finally cooled from 3500 K to 10 K and optimized. All calculations with amorphous SiO_2 were conducted with constant temperature and volume conditions. Charges, used in the reax force field for calculation of energy were extracted in order to characterize atom bonding in the silicon–silicon oxide interfaces. The unit cell dimensions, silicon layer thickness and total number of atoms in unit cells are shown in Table 1 and ideal model interfaces are shown in figure 1.

Table 1: Parameters of model systems used in simulations of Si–$cSiO_2$ interfaces. All unit cells are orthorhombic. N is number of atoms in a unit cell; s is thickness of a silicon layer; Δx and Δy are mismatches in x and y directions.

Silicon oxide (model)	Silicon surface	Unit cell size/Å	N	s/Å	Δx (SiO_2)	Δy (SiO_2)	Δx (Si)	Δy (Si)
β crystoballite ($cSiO_2$[110]A)	[110]	30.40×30.40×34.28	2124	7.9	2.3%	3.8%	-2.7%	-7.3%
β crystoballite ($cSiO_2$[110]B)	[110]	30.40×30.40×49.09	3024	8.2	2.2%	2.5%	-9.1%	-2.7%
β quartz ($qSiO_2$[110]A)	[110]	22.17×18.46×29.80	864	7.9	0.05%	7.2%	4.1%	-22.2%

β crystoballite ($cSiO_2$[111])	[111]	30.40×20.27×36.48	1416	6.9	-0.2%	-1.1%	0.6%	2.4%
β quartz ($qSiO_2$[111]A)	[111]	34.12×20.36×41.32	2136	6.9	-9.3%	-11.1%	0.8%	-27.9%
β quartz ($qSiO_2$[111]B)	[111]	30.31×23.19×40.81	2136	6.9	2.0%	4.4%	-11.6%	-12.3%
β quartz ($qSiO_2$[110]B)	[110]	36.81×42.63×28.34	3200	7.5	7.4%	7.7%	-13.4%	-5.5%
β quartz ($qSiO_2$[110]C)	[110]	44.34×36.99×29.55	3392	8.1	0.0%	7.9%	4.6%	-17.8%

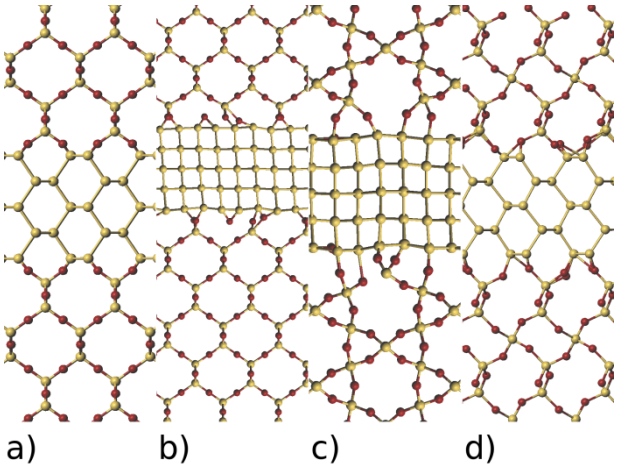

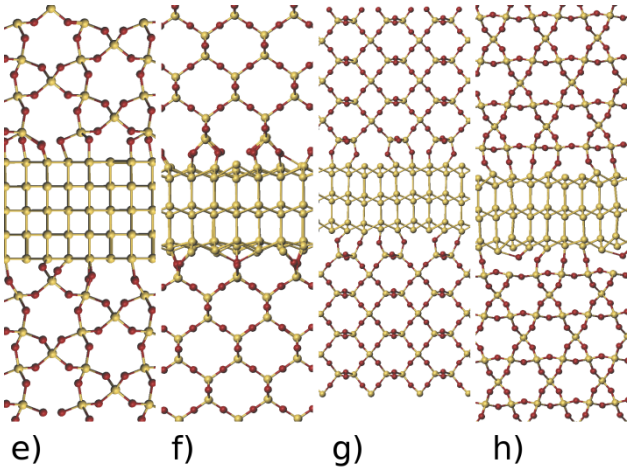

Figure 1. Model systems of the ideal interfaces between silicon and silicon oxide layers. a) $cSiO_2$[110]A; b) $cSiO_2$[110]B; c) $qSiO_2$[110]A; d) $qSiO_2$[110]B; e) $qSiO_2$[110]C f) $cSiO_2$[111]; g) $qSiO_2$[111]A; h) $qSiO_2$[111]B

Interesting bonding motifs are characterized by isolation of the region in the model systems that contain the motif of interest, and all atoms that resulted in unsatisfied valencies by the process of cutting are satisfied by attaching hydrogen atoms. That isolated systems were first optimized on MP2/6-31G(d) level by freezing all atoms except the added hydrogen atoms. After that, the system was reoptimized with all atoms freezed except few atoms, involved in the structural motif of interest. The constraints, put by frozen atoms mimic the constraints, implied by a crystal lattice. The optimization on high-level *ab-initio* calculation was used in order to check bonding and structural motifs independently of $ReaxFF_{SiO}$ parameterization. These calculations were done by using GAMESS program package.[31]

In order to quantify stress in silicon and silicon oxide slabs, the stress was calculated by using the definition of Daruka at al.[32] from the forces obtained with $ReaxFF_{SiO}$. In order to gain further insight in the nature of stress in interfaced systems, *ab-initio* calculations were made with molecular clusters, cut from the silicon and silicon oxide crystal lattices. These clusters are shown in figure 2. All frontier

atoms are decorated with hydrogen atoms in order to satisfy valencies on all atoms. Optimized structures were deformed (compressed/stretched) along *z* axis and gradients and energies were calculated on these deformed structures. Optimized structures are stretched and compressed up to 10 % along *z* axis. Silicon and cristobalite models were constrained to the C_{2v} symmetry and the tridimyte model was constrained to two different symmetries: C_3 and D_{3d} respectively. These constraints don't allow large change in geometries during optimizations. Unfortunately, no small representation of the quartz structure could be made, that can be optimized into a structure still similar to the initial quartz structure.

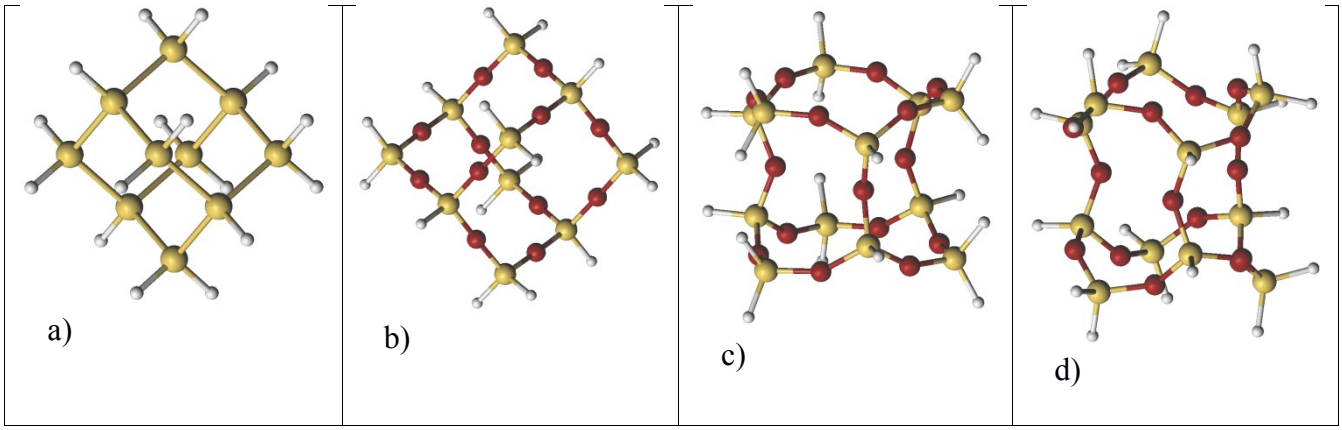

Figure 2. Modeled systems used in calculation of stress level caused by deformation. a) silicon; b) β-cristobalite; c) β-tridymite-D_{3d} constrained; d) β-tridymite-C_3 constrained

Results and discussion

Different models for the interfaces between silicon surfaces and different forms of silicon oxide are created in order to characterize bonding in these interfaces and to check their stability. Unlike the

models with Si[100] surface[25], all silicon atoms at the Si[110] and Si[111] surfaces have only one unsatisfied valency and in the case of Si[111] surface these atoms are separated by a relatively large distance, so oxygen atoms can't bridge them. Since oxygen atoms, that are inserted between silicon atoms in the first layer at the Si[100] surface lower the number of free valencies at Si[100] surface, the number of valencies available for bonding with SiO_2 in Si[100] surface is lower than in Si[110] and Si[111] surfaces. That results in dangling bonds in Si[110] and Si[111] interfaces. In some models ($cSiO_2$[110]B, $qSiO_2$[110]B), dangling bonds were removed by inserting bridging oxygen atoms (Figure 1 b and c), however inserting a bridging oxygen atom, requires rearrangements in bonding which results in the strain in the systems. Also, inserting bridging oxygen atoms makes strained three-(Si-Si-O) and four-(Si-Si-Si-O) member rings. Therefore we considered both, the systems with (Figure 1 b, c) and without (Figure 1 a, e) these bridging oxygen atoms. Unfortunately, there are models in which all atoms can't be valence-satisfied.

As in our previous paper, we used β-quartz instead of it's more stable α form, since β-quartz is more stable at elevated temperatures[33], that are used in simulations of thermal treatment. Simulations of thermal treatment of modeled systems were performed in order to change bonding in the interface region and the sequence of heating and annealing procedures was used to drive systems to the thermodynamically more stable state. In all systems, heat treatment didn't disrupt the structures of the silicon and the silicon oxide layers. The only difference between initial and annealed models is in dislocated oxygen atoms and in the bonding layout in the interface region.(figure 3)

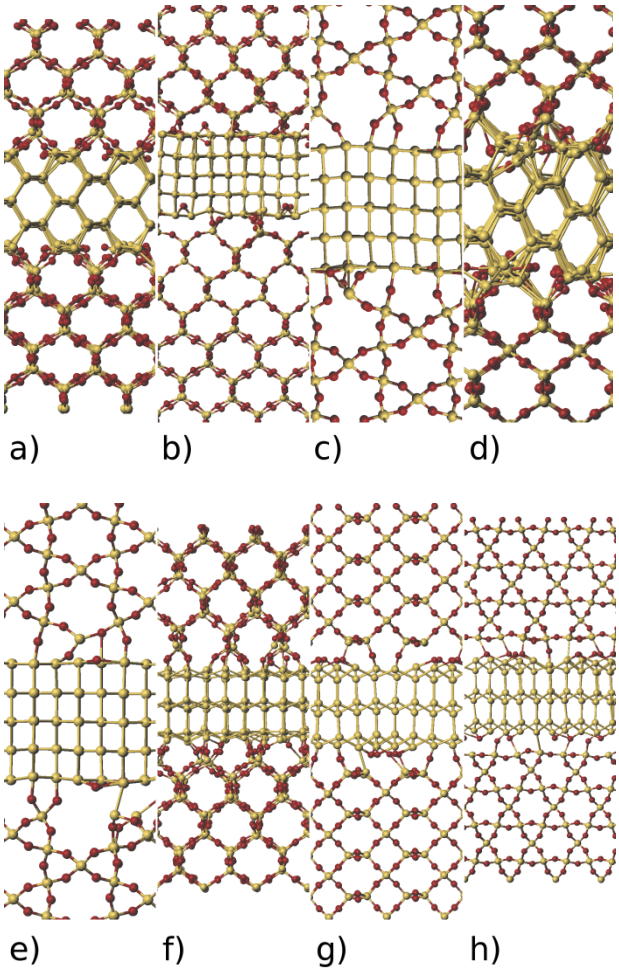

Figure 3. The structures of the modeled interfaces after simulation of thermal treatment. a) $cSiO_2$[110]A; b) $cSiO_2$[110]B; c) $qSiO_2$[110]A; d) $qSiO_2$[110]B; e) $qSiO_2$[110]C f) $cSiO_2$[111]; g) $qSiO_2$[111]A; h) $qSiO_2$[111]B

Unlike the case of interface between cristobalite and Si[100] surface[25] no interface considered in this work, has been reorganized into the amorphous two-dimensional layer. However, two of the considered models have a significant mismatch in periodic constants between two layers. In one case ($qSiO_2$[110]A) a mismatch creates buckling of the silicon layer that shapes the layer into a wavelike pattern. (Figure 4a) That buckling is caused by introduction of oxygen atoms at the surface of the

silicon layer and supported by the arrangement of atoms in the quartz layer. That arrangement pulls the silicon layer along the *z* coordinate in one direction, and on the other spot push the silicon layer into another direction. The another case is $qSiO_2$[111]B, where a high strain between layers is supported by oxygen atoms that migrated from the surface of β-quartz to the surface of the silicon layer, where dangling bonds were present. In that case, oxygen atoms are migrating from the SiO_2 layer, towards the dangling bonds, leaving Si-Si bonds behind. These oxygen atoms are inserted between silicon centers with unsatisfied valencies making one bond, that is the regular silicon-oxygen bond (about 1.8 Å) and two bonds that are strained (over 2.0 Å), partial bonds. (Figure 4b) Although silicon centers with dangling bonds are too far away for bridging by oxygen atoms, in strained systems that bridging is possible, although the bonds involved in bridging are elongated.

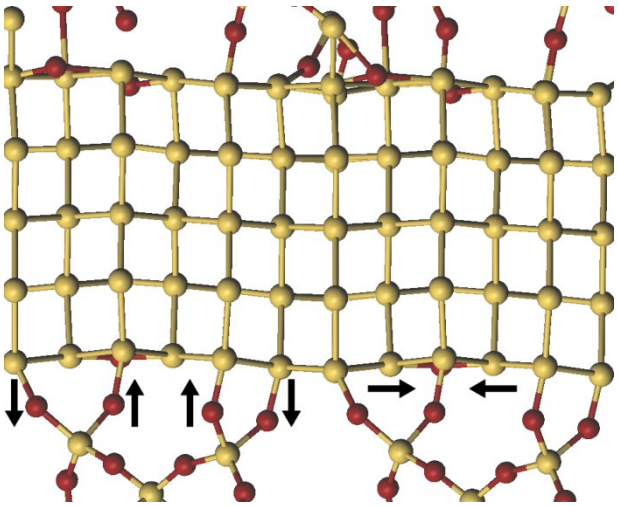

a)

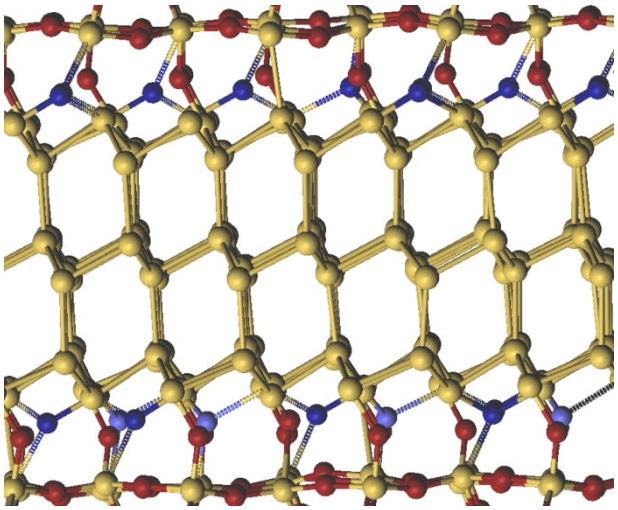

b)

Figure 4. a) Buckling of silicon layer. Buckling is caused by compression from the oxygen atoms at the surface of silicon layer (horizontal arrows) and from pulling and pushing from the quartz layer (vertical arrows). b) Compression stabilization of the silicon layer, caused by displaced oxygen atoms. Displaced oxygen atoms are shown in blue color and partial bonds are shown as stippled cylinders. The atoms that are only partially involved in bridging the atoms in the silicon layer are depicted in light blue.

In all interfaces, after simulation of thermal treatment, the reconstruction of the interfaces generates defects in form of three-coordinated [Si(3)] silicon atoms, (dangling bond)[20-22,34-37] five coordinated silicon atoms (floating bond)[38-40], threefold-coordinated oxygen atom[41,42] or displaced oxygen atom[42].

The nature of three-coordinated oxygen atoms in the strained interface (figure 4b) is further analyzed on model molecules, taken from the interface. The detailed analysis of the bonding in that strained systems is done by searching for energy minimum among the geometries with different positions of displaced oxygen atom. The search for energy minimum is done by optimization with high-level *ab*-

initio MP2/6-31G(d) calculations. All possible geometries where the oxygen atom makes bridges between silicon atoms are tried as potential candidates for the potential energy surface minimum, however all these geometries converged into the unique geometry (figure 5).

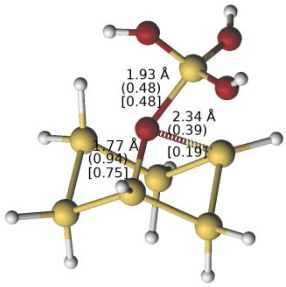

Figure 5. The optimized model for interaction of oxygen atom with three dangling bonds. Bond lengths (in Ångströms) are shown next to the bonds, bond orders calculated with ReaxFF$_{SiO}$ are shown in parenthesis and bond orders, calculated according to Mayer definition, at MP2/6-31G(d) level are shown in square brackets.

In this geometry, the oxygen atom is positioned asymmetrically between the three silicon atoms, so the bond lengths between them are different. The identical bonding pattern is obtained from the optimization by the ReaxFF$_{SiO}$. The bonding pattern, obtained with the *ab-initio* calculations, also confirms the finding obtained by optimization with the ReaxFF$_{SiO}$ where the oxygen atom makes three bonds with three different bond orders. The large number of five-coordinated silicon atoms is the result of the parameterization of the ReaxFF$_{SiO}$. The optimization of the small models with five coordinated Si atoms, taken from the ReaxFF$_{SiO}$ optimized interfaces, resulted in migration of oxygen atom into the Si-Si bond and in change in bonding pattern. (Figure 6) The end-result is a regular four-coordinated silicon atom. Therefore, this type of defect is an artifact of the ReaxFF$_{SiO}$. Most of the five-coordinated silicon atoms are the result of interaction with oxygen atom over an elongated, partial bond. The sum of

all bond orders on silicon atom in Si(5) defect is about 4 since most of the bonds around that atom have partial character.

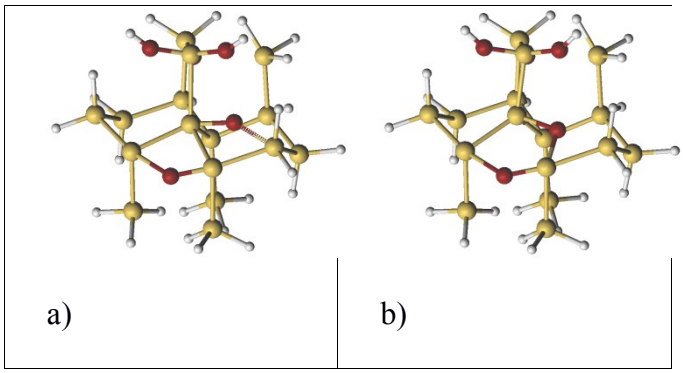

Figure 6. The overcoordinated silicon atom at the interface of Si110 with cristobalite. a) geometry optimized by the ReaxFF; b) the same geometry optimized by MP2/6-31G(d).

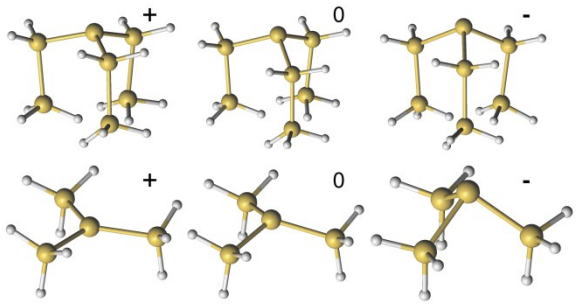

Figure 7. A model for Si(3) defect. The upper row shows atoms around Si(3), taken from the interface model and optimized with constraints; the lower row shows optimized *tris*(*trimethylsilyl*)*silane* without constraints. Charges of the models are shown next to it.

The large number of Si(3) atoms (P_b centers) at interfaces with β-cristobalite is a consequence of the great number of unsatisfied valencies at the surface of silicon slab that couldn't be rebonded with

oxygen atom from the surface of β-cristobalite. All initial silicon atoms with dangling bonds are pyramidal, as in silicon crystal, but with one bond missing. Thermal treatment and optimizations by the $ReaxFF_{SiO}$ leaves that silicon atom in the pyramidal coordination, although thermal treatment deforms the coordination from the ideal pyramidal structure.

The dangling bond in silicon layer can trap electrons or holes[21,23] resulting in positive (P_b^+) or negative (P_b^-) charge. Weather P_b center is positive or negative, depends on the Fermi level. According to Lenahan and Conley[23], the low Fermi level makes Si(3) unpopulated with electrons making it positive, P_b^+; in intermediate levels P_b center is populated with the single electron, and at the high Fermi level has two electrons and is negative: P_b^-. Unfortunately, the $ReaxFF_{SiO}$ was parameterized for a neutral silicon only[27] and it can't describe P_b^+ and P_b^-. Therefore, the structure of Si(3) atom was also optimized inside a representative cluster (Si_7H_{15}) by using *ab-initio* calculations. The same clusters with the positive and negative charge were also optimized. The result is shown in figure 7. Silicon atoms with the positive charge tend to migrate toward the planar configuration, and silicon atom with the negative charge makes more sharped angle pyramid. Since the silicon atoms around the pyramidal atom were constrained, the geometries of modeled Si(3) defects on figure 7 could be the result of steric conditions coming from the bond-length of Si-Si bonds. Therefore, the geometries of *tris*(*trimethylsilyl*)*silane radical* (Si_4H_9) (figure 7, the lower row) were also optimized without constrictions in order to check the defect geometry in fully relaxed structures. The presented structures show the same trend as in the constrained structures (figures 7, the upper row), although the differences between the structures with different charges are much more pronounced. In the structure with the positive charge the Si(3) atom lies almost in the plane with three neighboring silicon atoms. In order to check whether this out-of-plain deviation is an artifact, caused by the insufficient geometry convergence threshold, the geometry was reoptimized with the threshold decreased by an order of

magnitude (10^{-5} Hr/Bohr for the largest component of gradient and 3.33 10^{-6} Hr/Bohr for RMS gradient). In separate calculation, the geometry of positively charged model for Si(3) atom is optimized from the initial geometry in which all silicon atoms lie in the plain. All mentioned calculations converged into a pyramidal geometry shown in figure 7. There is no significant difference between geometries of pyramidal three-coordinated silicon atoms in the interface, obtained by the $ReaxFF_{SiO}$ and the neutral three-coordinated silicon atom in constrained model molecule, optimized with MP2/6-31G(d). In the negatively charged constrained model, Si-Si bonds are about the same length as in negative unconstrained models. Si-Si bonds tend to be shorter as charge increases toward positive values. The reason for this trend is a tendency of a three-coordinated silicon atom toward large-angle pyramidal structures. Since the base of pyramid is constrained, the large-angle pyramid is achieved by shortening Si-Si bonds.

The relative energies of the calculated models show that the negatively charged structures are the most stable (Table 2). This makes the trend in energies: $Si(3)^- < Si(3)^0 < Si(3)^+$ which is opposite from the trend published by Lenahan at al.[23] Conclusions about the change of populations by Lenahan and Conley were drawn from EPR spectra and only a neutral form is EPR active, so there was no indication that $Si(3)^+$ should be more stable than $Si(3)^0$. Furthermore the same trend as ours is observed in calculations of Si(3) with interaction with oxygen atoms by Blochl[43].

Table 2: The geometrical parameters of three-coordinated silicon atoms, obtained with the $ReaxFF_{SiO}$ in the modeled interface and with MP2/6-31G(d) in model molecules. The geometrical parameters are: h: the pyramid height, r_{Si-Si}: the silicon-silicon bond length; ΔE is the difference in energy with respect to the uncharged model.

structure	h/Å	r_{Si-Si}/Å	ΔE/eV

Interface, ReaxFF$_{SiO}$	1.04*	2.30*	
$Si_7H_{15}^+$	0.79*	2.20*	7.34*
$Si_7H_{15}^0$	1.01*	2.29*	0 (reference)
$Si_7H_{15}^-$	1.21*	2.38*	-2.42*
$Si_4H_9^+$	0.10	2.38	6.94
$Si_4H_9^0$	0.48	2.34	0 (reference)
$Si_4H_9^-$	1.27	2.36	-1.74

*the average value

There are two uncertainties about the stabilities of P_b in Si-SiO_2 interface. The first uncertainty is in the charge on P_b defect. The energies, calculated with *ab-initio* calculations are obtained from small models while real P_b centers are located on the much larger systems where the charge can be delocalized and effectively alter the charge on three-coordinated silicon atom. Nonetheless, it was shown[44-46] that the charge can accumulate on defects at Si-SiO_2 interface similarly as in localized models. The second uncertainty is in the electric field between silicon and silicon-oxide layers. The electronegativity of oxygen atoms in SiO_2 layer withdraws the charge making that layer more negative than the silicon layer. The electric field is also contributed by local charges on three-coordinated Si atom and point charges within the SiO_2 layer. The charges on the ideal Si-SiO_2 interface were estimated from the electron-equilibration method and from *ab-initio* calculations on clusters to about 0.01 Hr e^{-1} $Bohr^{-1}$.[47,48] In order to check the relative stability of three-coordinated silicon atoms in the electric field, we optimized models (Si_7H_{15} and Si_4H_9) in the electric field with different strengths. As can be seen in figure 8, the differences in energy between charged and neutral Si_7H_{15} decreases as

electric field increases. At the strongest field, used in calculations, differences in energy are still much larger than the differences in Fermi level where change in occupations of charged P_b defects was observed.[23] That indicates that the charge in the defect is delocalized, and only partially on Si(3), making it effectively less charged and/or the strength of the electric field felt by Si(3) is stronger than the estimated value. Unfortunately, strong electric fields cause instability in SCF convergence, so calculations with stronger electric fields weren't done.

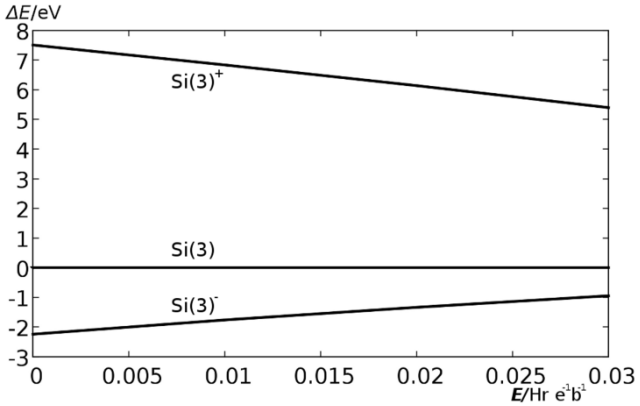

Figure 8. The relative stability (ΔE) of positive [$Si(3)^+$] and negative [$Si(3)^-$] three-coordinated silicon with respect to the neutral form [$Si(3)^0$] atom in modeled interfaces with respect to the electric field ($\boldsymbol{E}$).

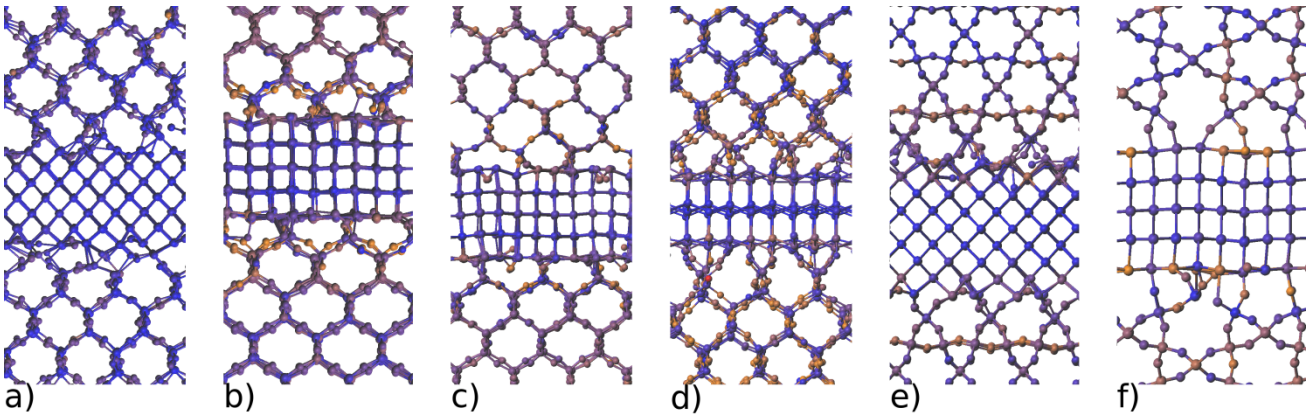

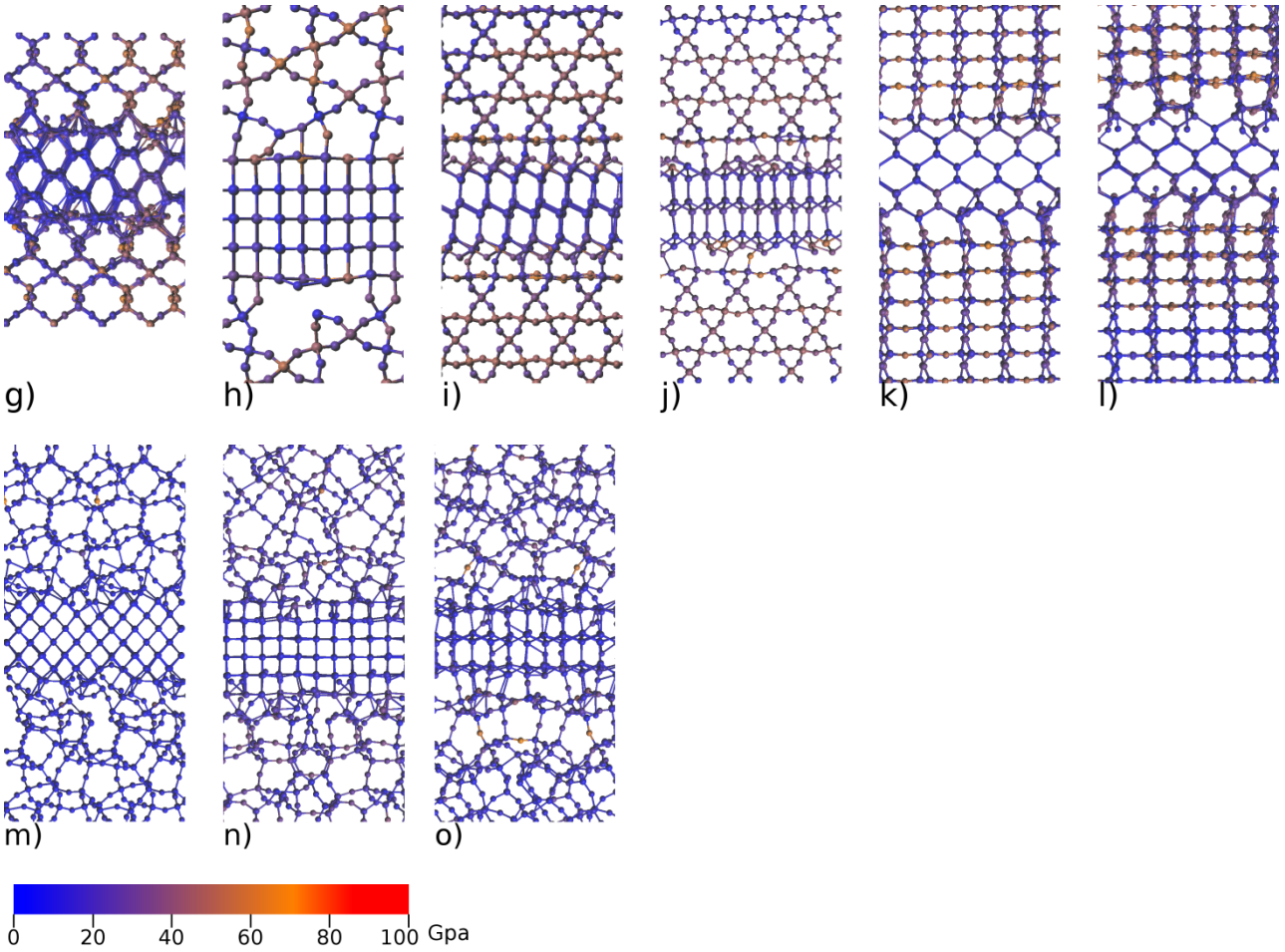

Figure 9. The stress in the layers of interfaced slabs of silicon and silicon-oxide. a) $cSiO_2$[100]; b) $cSiO_2$[110]A; c) $cSiO_2$[110]B; d) $cSiO_2$[111]; e) $qSiO_2$[100]; f) $qSiO_2$[110]A; g) $qSiO_2$[110]B; h) $qSiO_2$[110]C; i) $qSiO_2$[111]A; j) $qSiO_2$[111]B; k) $tSiO_2$[100]cb; l) $tSiO_2$[100]r; m) $aSiO_2$[100]; n) $aSiO_2$[110]; o) $aSiO_2$[111]

The color-coded root-mean-square stress tensor is shown in figure 9 for each atom in modeled systems. The Si[100]-cristobalite interface shows a very little stress.(Figure 9a) This result is in accordance with our previous results[25] where bond lengths in this interface were found to be closest to the bond lengths in the ideal crystals. The bonding pattern in this interface is also found to be the most

disturbed among Si[100] interfaces. This interface is also more disturbed than any interface with crystalline silicon, considered in this paper. In most interfaces, the greatest strain is in the region of silicon oxide, next to the interface. (9 b, c, e, f, i, j) Further from the interface, level of strain drops. In interfaces with relatively large difference in lattice constants (figure 9 i, j, k, l), the greatest strain is located on Si-O bonds in the silicon-oxide layer that is oriented parallel to the interface. The exception is the interface between Si[111] and quartz where the silicon slab is buckled. (Figure 9f) In that interface the strain is greatest in the areas where oxygen atoms are inserted in the silicon surface. In that case, the dominant strain pattern in the silicon oxide layer is vertical with respect to the direction of the silicon slab since the bonding pattern between silicon and silicon oxide makes silicon slab bending. In tridymite-Si[100] (Figure 9 k, l) the greatest stress is on oxygen atoms, that are coordinated almost linearly, parallel to the interface. In that interface there is a significant mismatch (about 12%) in lattice constants of silicon and tridymite.

In each system considered, the silicon layer is less stressed than silicon oxide layers, despite the relatively large stress values in some cases of silicon oxide. The difference in stress values in silicon and silicon oxides is analyzed on the model systems of silicon and silicon-oxide. The calculation of energy gradients on these modeled systems revealed that stretching or compressing a silicon slab results in much lower forces than applying the same deformations on silicon oxide slabs. Figure 10 shows the energy gradient in the model clusters (Figure 2) (which is proportional to the stress), as a function of deformation. This explains a very low stress in silicon slabs sandwiched with silicon oxide layers. The large forces in deformed silicon-oxide are the consequence of much deeper and steeper potential well for dissociation of Si-O bond than potential well of the Si-Si bond.[27]

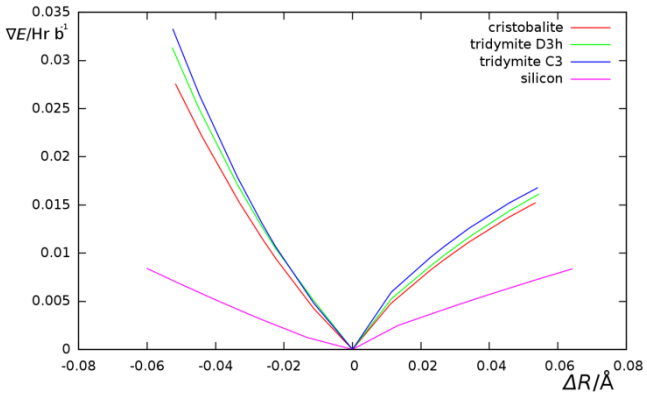

Figure 10. The energy gradients on the deformed model systems that represent silicon and silicon oxide crystals. Deformations are represented as a mean bond length (*R*) stretching (positive values) or compressing (negative values).

The lowest stress is in the systems with amorphous SiO_2. These systems don't have constraints in lattice constants as in cases of crystalline SiO_2. Instead of a stress in preferred directions, a large stress in amorphous systems is localized on isolated atoms. On average, the stress is much lower in amorphous systems (under 8 Gpa) which is in accordance with calculations of Khalilov and al..[49]

In our last article we used atom charges[25] as a convenient method for determination of the position of silicon atoms with different oxidation states. Silicon atoms that are connected to more oxygen atoms (more positive oxidation number) have a more positive charge since oxygen atoms drain charge by the electronegativity effect. The charges of silicon atoms with particular oxidation number are given in table 3. The exact charges may vary from these values since deformations in the coordination sphere can also make an influence. This effect is pronounced in the $cSiO_2$[110]A and the $qSiO_2$[110]B interfaces (figure 11a and c) where the stress causes spreading of charges in the SiO_2 layer. Furthermore, we showed that in the interface region of cristobalite and Si[100] there is no grouping of silicon atoms with the same oxidation number to the same *z* coordinate, indicating that the crystalline

order is disrupted.[25] This amorphous order is confined only to the interface regions. Here, we repeated the analysis on the Si[110] and Si[111] interfaces with crystalline SiO_2 as well as on the interfaces with amorphous SiO_2. (Figure 11 and Figure S1 in supplement)

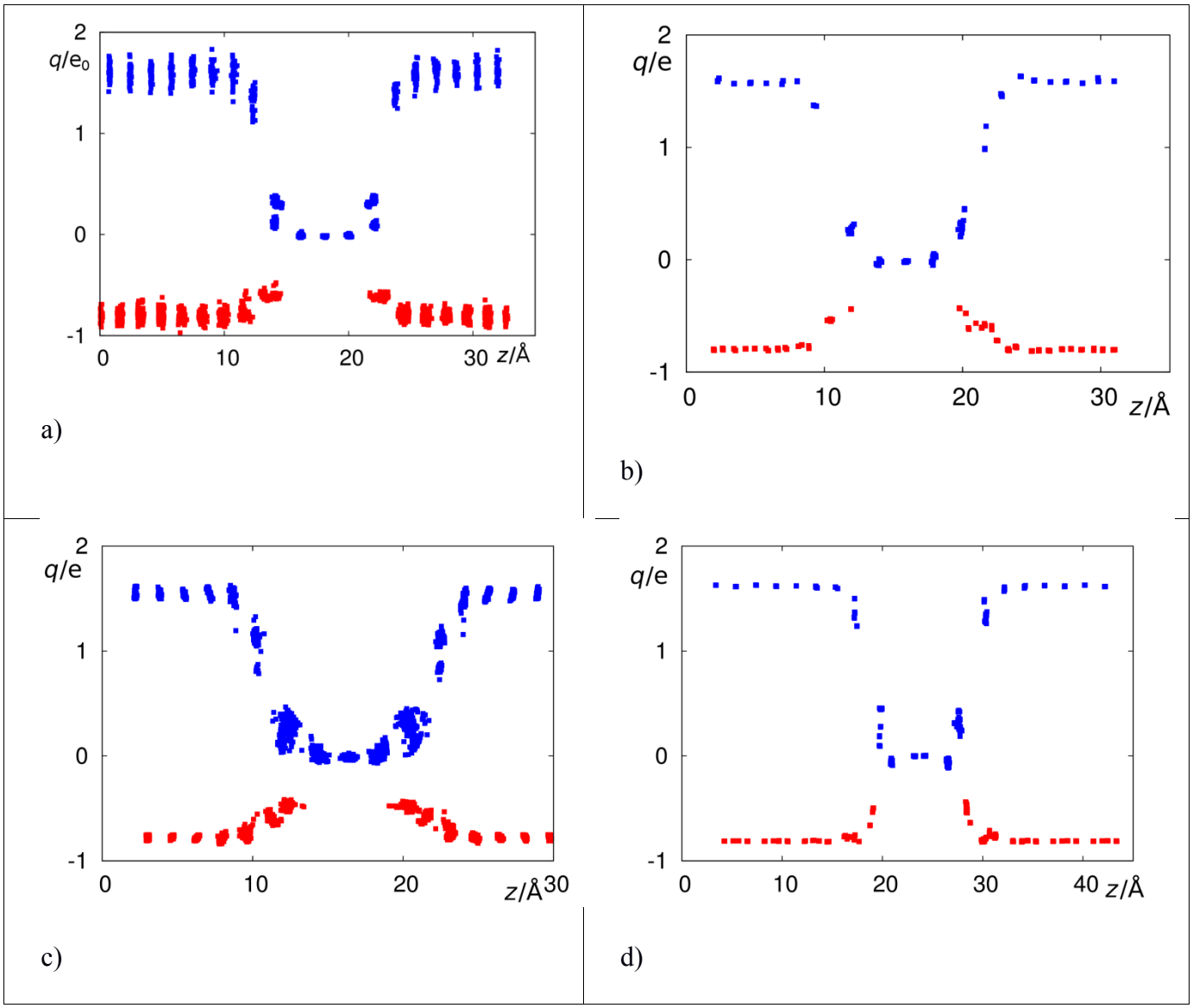

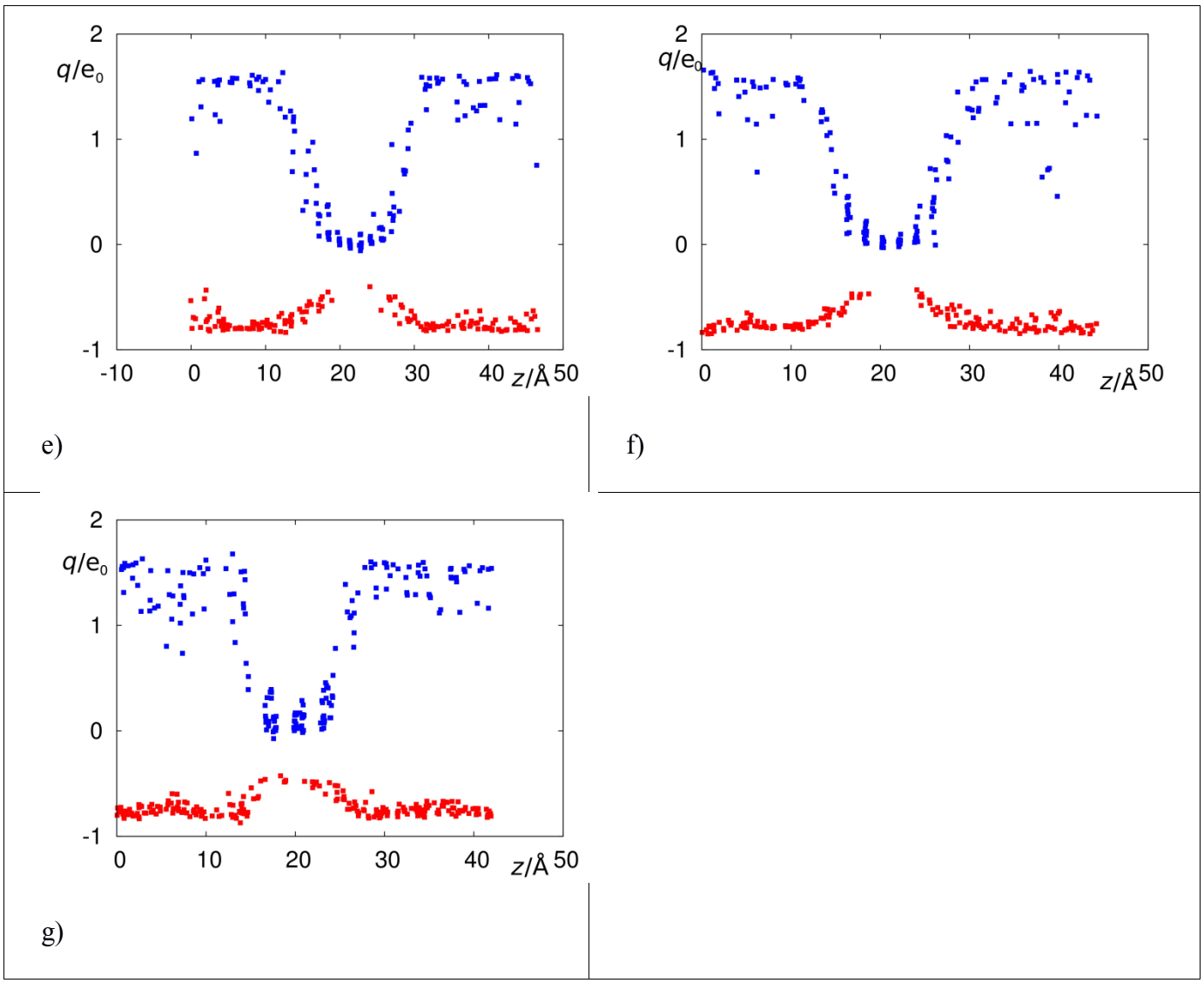

Figure 11. The atomic charges in the modeled systems; Atomic charges of silicon atoms are shown in blue color and oxygen charges in red color; a) $cSiO_2$[110]A, b) $qSiO_2$[110]A, c) $qSiO_2$[110]B, d) $qSiO_2$[111]A e) $aSiO_2$[100], f) $aSiO_2$[110], g) $aSiO_2$[111].

All interfaces with crystalline SiO_2 are well defined with distinctive layers of silicon atoms with different oxidation numbers. The structure of $qSiO_2$[110]B is disrupted more than other interfaces with

Si[110] and Si[111] which is manifested in a larger spread of charges. In that case there is also a large deformation in silicon layer as can be seen from a large spread of atomic positions at the center of figure 11c. The deformation is also visible in figure 3d. The large spread of atomic positions caused merging of the layers occupied by atoms with oxidation number 0 and 1. Atomic charges at interfaces with $aSiO_2$ show continuous change from 0 in silicon layer to about +1.6 e in $aSiO_2$ layer. This is consistent with the charges we obtained in the case of interface $cSiO_2[100]$[25]. Figures 11e-g indicate that there are silicon atoms in $aSiO_2$ layer with oxidation number lower than +4. That is a consequence of stray Si-Si bonds in that layer.

Table 3: Charges of silicon atoms in $Si-SiO_2$ system with the different oxidation number. Charges are estimates since exact values can vary, depending on deformations in the coordination sphere.

oxidation number	charge
0	0
+1	0.3
+2	0.8
+3	1.1
+4	1.6

Conclusion

The analysis of bonding patterns in models of interfaces with Si[110] and Si[111] surfaces with different forms of silicon oxide have shown that a large number of dangling bonds can produce three-

coordinated oxygen atoms with partial bond orders. These three-coordinated oxygen atoms are the result of a strained system since the oxygen atoms couldn't bridge silicon atoms otherwise. Introducing the bridging oxygen atoms at the quartz-Si[110] interface can reduce the stress at the interface by buckling of the silicon layer. Defects in form of three-coordinated silicon atoms, analyzed on small modeled systems are most stable as negatively charged. Introduction of the electric field, caused by the interface, reduces the stability of negatively charged three-coordinated silicon atom. The stress in the Si-SiO_2 systems is mostly contained in SiO_2 layer. In systems with a large mismatch in periodic constants, where bonding in SiO_2 layer is parallel to the interface, the stress is significantly contributed by these bonds. In system where silicon layer is buckled, the greatest stress is near the oxygen atom that caused buckling. The analysis of susceptibility for stress showed that silicon has lower stress than silicon-oxide if put under the same strain. Calculation of charges of silicon atoms showed that none of interfaces between crystalline silicon and crystalline SiO_2 show disorder in positions of silicon atoms with the same oxidation number as in interfaces with aSiO_2.

Acknowledgment

The authors wish to thank to Adri van Duin for giving the ReaxFF_{SiO} parameters. This studz has been partiallz funded bz EU project NanoPV (FP7-NMP3-SL-2011-246331).

References

1. Cahn, R. W. *Electrochem. Soc. Interface* **2005**, 14, 15-16.

2. Latyshev, A. V.; A. L. Aseev, *Uspekhi Fizicheskikh Nauk*, **1998**, 168, 1126-1127.

3. Diebold, A. C.; Venables, D; Chabal, Y.; Muller, D.; Weldon, M.; Garfunkel, E. *Mater. Sci. Semicond. Proc.* **1999**, 2, 103-147.

4. Ieong, M.; Doris, B.; Kedzierski, J.; Rim, K.; Yang, M. *Science* **2004**, 306, 2057-2060.

5. Wilk, G. D.; Wallace, R. M.; Anthony, J. M. *J. Appl. Phys.* **2001**, 89, 5243–5275.

6. Chabal, Y. J.; Feldman, L. C. *Electrochem. Soc. Interface* **2005**, 14, 31-34.

7. Akatsu, H.; Sumi, Y.; Ohdomari, I. *Phys. Rev. B* **1991**, 44, 1616-1621.

8. Ourmazd, A.; Taylor, D. W.; Rentschler, J. A. *Phys. Rev. Lett.* **1987**, 59, 213-216.

9. Munkholm, A.; Brennan, S.; Comin, F.; Ortega, L. *Phys. Rev. Lett.* **1995**, 75, 4254-4257.

10. Robinson, I. K.; Waskiewicz, K.; Tung, R. T. *Phys. Rev. Lett.* **1986**, 57, 2714-2717.

11. Takahashi, I.; Shimura, T.; Harada, J. *Phys.: Condens. Matter.* **1993**, 5, 6525-6536.

12. Himpsel, F. J.; McFeely, F. R.; Taleb-Ibrahimi, A.; Yarmoff, J. A. *Phys. Rev. B* **1988**, 38, 6084-6096.

13. M. M. Banaszak Holl, McFeely, F. R. *Phys. Rev. Lett.* **1993**, 71, 2441-2444.

14. Korkin, A.; Greer, J. C.; Bersuker, G.; Karasiev, V. V.; Bartlett, R. J. *Phys. Rev. B* **2006**, 73, 165312.

15. Helms, C. R.; Poindexter, E. H. *Rep. Prog. Phys.* **1994**, 57, 191-852.

16. Kageshima, H.; Shiraishi, K. *Phys. Rev. Lett.* **1998**, 81 5936-5939.

17. Caplan, P. J.; Helbert, J. N.; Wagner, B. E.; Poindexter, E. H. *Surf. Sci.* **1976**, 54, 33–42.

18. Chung, M. F.; Haneman, D. *J. Appl. Phys.* **1966**, 37, 1879-1890.

19. Nishi, Y. *Japan. J. Appl. Phys.* **1971**, 10, 52-62.

20. Cook, M.; White, C. T. *Phys. Rev. Lett.* **1987**, 59, 1741-1744.

21. Cook, M.; White, C. T. *Phys. Rev. B* **1988**, 38, 9674-9685.

22. Stirling, A.; Pasquarello, A.; Charlier, J.-C.; Car, R. *Phys. Rev. Lett.*, **2000**, 85, 2773-2776.

23. Lenahan, P. M.; Conley J. F., Jr. *J. Vac. Sci. Technol. B* **1998**, 16, 2134-2153.

24. Street, R. A.; Mott, N. F. *Phys. Rev. Lett.* **1975**, 35, 1293-1296.

25. Kovačević, G.; Pivac, B. *Phys. status solidi A* **2012**, 210, 717–722.

26. van Duin, A. C. T.; Dasgupta, S.; Lorant, F.; Goddard, W. A., III. *J. Phys. Chem. A* **2001**, 105, 9396-9409.

27. van Duin, A. C. T.; Strachan, A.; Stewman, S.; Zhang, Q.; Xu, X.; Goddard, W. A., III. *J. Phys. Chem. A* **2003**, 107, 3803-3811.

28. Fogarty, J. C.; Aktulga, H. M.; Grama, A. Y.; van Duin, A. C. T.; Pandit, S. A. *J. Chem. Phys.* **2010**, 132, 174704.

29. van Ginhoven, R. M.; Jónsson, H.; Corrales, R. L. *Phys. Rev. B* **2005**, 71 024208

30. van Ginhoven, R. M.; Hjalmarson, H. P. *Nucl. Instr. and Meth. in Phys. Res. B* **2007**, 255, 183–187.

31. Schmidt, M. W.; Baldridge, K. K.; Boatz, J. A.; Elbert, S. T.; Gordon, M. S.; Jensen, J. J.; Koseki, S.; Matsunaga, N.; Nguyen, K. A.; Su, S.; et al. *J. Comput. Chem.* **1993**, 14, 1347-1363.

32. Daruka, I.; Barabási, A.-L.; Zhou, S. J.; Germann, T. C.; Lomdahl, P. S.; Bishop, A. R. *Phys. Rev. B* **1999**, 60, R2150-R2153.

33. Shapiro, S. M.; O' Shea, D. C.; Cummins, H. Z.; *Phys. Rev. Lett.* (1967), **19**, 361-364.

34. Stesmans, A. *Appl. Phys. Lett.* **1986**, 48, 972-975.

35. Füssel, W.; Schmidt, M.; Angermann, H.; Mende, G.; Flietner, H. *Nucl. Instr. Meth. Phys. Res. A* **1996**, 377, 177-183.

36. Luo, L.-B.; Yang, X.-B.; Liang, F.-X.; Xu, H.; Zhao, Y.; Xie, X.; Zhang, W.-F.; Lee, S.-T. *J. Phys. Chem. C* **2011**, 115, 18453–18458.

37. Ragnarsson, L.-Å.; Lundgren, P. *J. Appl. Phys.* **2000**, 88, 938-942.

38. Martin-Moreno, L.; Verges, J. A. *Phys. Rev. B*, **1989**, 39, 3445-3448.

39. Sanz-Navarro, C. F.; Kenny, S. D.; Smith, R. *Nanotech.* **2004**, 15, 692–697.

40. Biswas, R.; Pan, B. C.; Ye, Y. Y. *Phys. Rev. Lett.* **2002**, 88, 205502-1-4.

41. Pasquarello, A.; Hybertsen, M. S.; Car, R. *Nature* **1998**, 396, 58-60.

42. Richard, N.; Martin-Samos, L.; Roma, G.; Limoge, Y.; Crocombette, J.-P. *J. Non-Cryst. Solids* **2005**, 351, 1825–1829.

43. Blochl, P. E. *Phys. Rev. B* **2000**, 62, 6158-6179.

44. Kutsuki, K.; Ono, T.; Hirose, K. *Sci. Technol. Adv. Mater.* **2007**, 8, 204-207.

45. Ono, T. *Phys. Rev. B*, **2009**, 79, 195326-1-5.

46. Ben-Porat, C. H.; Cherniavskaya, O.; Brus, L.; Cho, K.-S.; Murray, C. B. *J. Phys. Chem. A*, **2004**, 108, 7814-7819.

47. Lucovsky, G.; Yang, H.; Massoud, H. Z. *J. Vac. Soc. Technol. B*, **1998**, 16, 2191-2198.

48. Massoud, H. Z. *J. Appl. Phys.* **1988**, 63, 2000-2005.

49. Khalilov, U.; Pourtois, G.; van Duin, A. C. T.; Neyts, E. C. J. Phys. Chem. C, 2012, 116, 21856−21863